

Stable Calculation of Optical Properties of Large Non-Periodic Dissipative Multilayered Systems

Luis Eduardo Puente-Díaz^{1,2}, Victor Castillo-Gallardo^{1,2,3},
Guillermo P. Ortiz⁴, José Samuel Pérez-Huerta⁵, Héctor
Pérez-Aguilar¹, Vivechana Agarwal³, and W. Luis Mochán²

¹Facultad de Ciencias Físico Matemáticas, Universidad Michoacana de San Nicolás de Hidalgo, Av. Francisco J. Múgica S/N 58030, Morelia, Mich., México.

²Instituto de Ciencias Físicas, Universidad Nacional Autónoma de México, Av. Universidad S/N, Col. Chamilpa, 62210 Cuernavaca, Morelos, México.

³Centro de Investigación en Ingeniería y Ciencias Aplicadas, Universidad del Estado de Morelos, Av. Universidad 1001 Col. Chamilpa, Cuernavaca, Morelos 62209, México.

⁴Departamento de Física, Facultad de Ciencias Exactas, Naturales y Agrimensura, Universidad Nacional del Nordeste, Av. Libertad 5460, 3400, Corrientes, Argentina.

⁵Unidad Académica de Ciencia y Tecnología de la Luz y la Materia, Universidad Autónoma de Zacatecas, Carretera Zacatecas-Guadalajara km. 6, ejido la Escondida, Campus UAZ Siglo XXI, Zacatecas, Zac. 98160, México.

February 2, 2022

Abstract

The calculation of the transfer matrix for a large non-periodic multilayered system may become unstable in the presence of absorption. We discuss the origin of this instability and we explore two methods to overcome it: the use of a total matrix to solve for all the fields at all the interfaces simultaneously and an expansion in the Bloch-like modes of a periodic artificially repeated system. We apply both methods to obtain the reflectance spectra of multilayered chirped structures composed of nanostructured porous silicon (PS). Both methods yield reliable and numerically stable results. The former allows an analysis of the field within all layers while the latter is much more efficient computationally, allowing

the design of novel structures and the optimization of their parameters. We compare numerical and experimental results across a wide spectral range from the infrared to the ultraviolet.

1 Introduction

Multilayered dielectric structures have been studied extensively in the visible (Vis) and near infrared (NIR) frequency ranges, as in these ranges these structures might have a small dispersion and dissipation, and might thus have a high reflectivity compared to that of metallic mirrors [1]. This high reflectivity may be achieved over a wide range of frequencies and angles of incidence and for both TE and TM polarization in what are known as omnidirectional mirrors (OM's) [1, 2]. The simplest and most common OM is a structure formed through the periodic repetition of a unit cell formed from two alternating layers with high and low refractive indices [1, 3]. There are many examples of these OM's designed for the Vis [4, 5, 6, 7] and NIR [1, 8, 9, 10] ranges. One common material for their manufacture is nanostructured porous silicon (PS), obtained from Si wafers through an electrochemical etching, a simple synthesis technique that does not require sophisticated equipment [11, 12]. This process allows a control of the refractive indices of the layers that make up our structure through the current density applied during the anodizing process. The thickness of the layers is controlled through the time during which this current is applied. Some works have reported omnidirectional dielectric mirrors composed of multilayered PS structures in which the index of refraction varies quasi-continuously according to a given functional dependence on the depth [13, 14]. Other have stacked two or more periodic structures, each composed of pairs of layers with different thicknesses [15, 16] yielding NIR OM's. Completely oxidized *chirped* multilayered structures, that is, multilayered structures where the thickness of successive pairs of layers is gradually increased [6], have also been developed for the Vis region.

The calculation of the optical properties of these systems is usually carried out through the use of transfer matrices [17, 18]. Each layer is characterized by a 2×2 matrix that transfers the continuous independent components of the electromagnetic field from one interface to the next. Multiplying the matrices of all the layers we obtain a transfer matrix that relates the fields at the first and last interfaces, where boundary conditions are applied to obtain the optical coefficients. Unfortunately, in the presence of dissipation, the simple product of transfer matrices may become unstable [19] and the resulting optical properties may be unreliable. This would be the case for chirped PS OM tuned to the ultraviolet range in which Si shows a non-negligible dispersion and dissipation. In order to attack this and similar cases, in this paper we explore two alternative methods to achieve numerical stability, reliability and computational efficiency.

The paper is organized as follows. In Section 2 we develop two alternative formalisms that allow the calculation of the optical properties of large multilayered structures even in the case where the ordinary transfer matrix method

fails; in Subsection 2.2 we present a formalism based on an extended matrix that allows calculating the fields at all interfaces, while in Subsection 2.3 we present a formalism based on an expansion on Bloch-like modes of an artificial periodically repeated structure from which the actual system is a finite slice. In Section 3 we provide experimental details about our manufacture of the porous silicon structures with which we test our formalism and in Section 4 we present and discuss numerical and experimental results. Finally, Section 5 is devoted to conclusions.

2 Theory

2.1 Transfer Matrix

Let us consider a system composed of N layers $j = 1 \dots N$ of width d_j and index of refraction n_j , as shown in Fig. 1, with interfaces lying on the xz plane and stacked along the z direction. The propagation of an electromagnetic wave in this system can be described by a 2×2 transfer matrix

$$\mathbf{M} = \mathbf{M}_N \mathbf{M}_{N-1} \dots \mathbf{M}_2 \mathbf{M}_1 \quad (1)$$

that relates the components parallel to the interfaces, E_{\parallel} and H_{\parallel} , of the electric and magnetic fields across the structure

$$\begin{pmatrix} E_{\parallel} \\ H_{\parallel} \end{pmatrix}_{z_N} = \mathbf{M} \begin{pmatrix} E_{\parallel} \\ H_{\parallel} \end{pmatrix}_{z_0}, \quad (2)$$

where we designate by z_{j-1} the lower and by z_j the upper interfaces of layer j , z_0 corresponds to the interface with the ambient of index of refraction n_0 , z_N to the interface with the substrate of index of refraction $n_s = n_{N+1}$, and \mathbf{M}_j relates the fields across a single layer, from z_{j-1} to z_j ,

$$\begin{pmatrix} E_{\parallel} \\ H_{\parallel} \end{pmatrix}_{z_j} = \mathbf{M}_j \begin{pmatrix} E_{\parallel} \\ H_{\parallel} \end{pmatrix}_{z_{j-1}}, \quad (3)$$

and is given by

$$\mathbf{M}_j = \begin{pmatrix} \cos k_j d_j & iZ_j \sin k_j d_j \\ iY_j \sin k_j d_j & \cos k_j d_j \end{pmatrix}, \quad (4)$$

where

$$k_j = \sqrt{\epsilon_j q^2 - Q^2} \quad (5)$$

is the z component of the wavevector for fields that move towards the z direction, Z_j is the corresponding surface impedance, $Y_j = 1/Z_j$ is the surface admittance, $\epsilon_j = n_j^2$ is the permittivity (for simplicity we assumed nonmagnetic media with permeability $\mu_j = 1$), $q = \omega/c = 2\pi/\lambda$ is the free-space wavenumber corresponding to the wavelength λ and Q is the projection of the wavevector onto the interfaces, which is conserved according to Snell's law and the law of

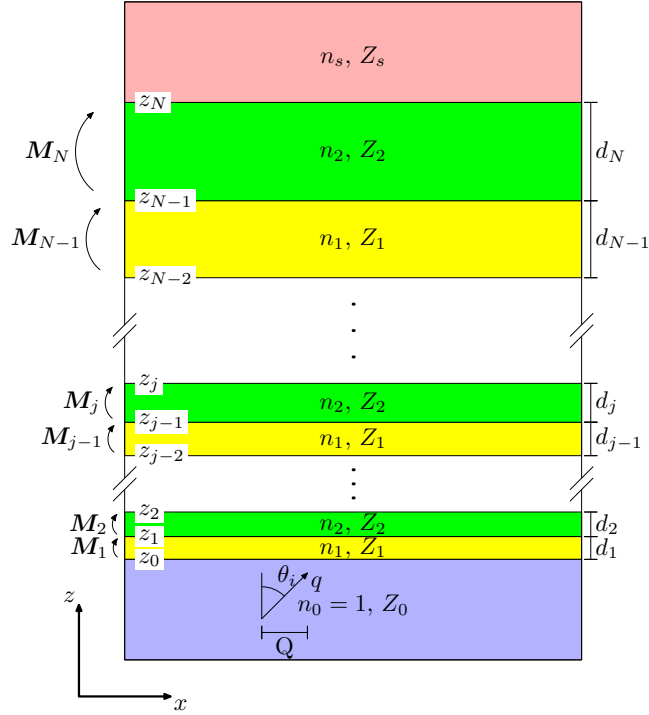


Figure 1: Multilayered system composed of N layers numbered $j = 1 \dots N$ with widths d_j and characterized by a transfer matrix M_j . Each layer is made of one or another of two alternating materials with indices of refraction n_1 and n_2 . The system is deposited on a substrate with index of refraction n_s and is illuminated from an ambient with index of refraction n_0 which we take as vacuum ($n_0 = 1$). All interfaces lie on the xy plane, the axis of the structure is along z and we took xz as the incidence plane. We indicate the height z_j of each interface, the wavevector of the incident field with wavenumber $q = \omega/c = 2\pi/\lambda$, incidence angle θ_i and parallel projection $Q = q \sin \theta_i$.

reflection, $Q = n_0 q \sin \theta_i$ with θ_i the angle of incidence. The surface impedances are given by $Z_j = q/k_j$ for TE polarization and $Z_j = k_j/q\epsilon_j$ for TM polarization.

By writing the fields at the ambient at z_0^- in terms of an incident and a reflected wave,

$$E_{\parallel}(z_0) = \begin{cases} 1 + r & \text{(TE)} \\ Z_0(1 - r) & \text{(TM)} \end{cases}, \quad H_{\parallel}(z_0) = \begin{cases} Y_0(1 - r) & \text{(TE)} \\ 1 + r & \text{(TM)} \end{cases}, \quad (6)$$

and writing the fields in the substrate at z_N^+ in terms of a transmitted wave

$$E_{\parallel}(z_N) = \begin{cases} t & \text{(TE)} \\ Z_s t & \text{(TM)} \end{cases}, \quad H_{\parallel}(z_N) = \begin{cases} Y_s t & \text{(TE)} \\ t & \text{(TM)} \end{cases}, \quad (7)$$

assuming an incident wave of unit amplitude, Eq. (2) becomes a system of two equations which may be solved for the two unknowns, the reflection and transmission amplitudes r and t .

2.2 Extended Matrix

The common procedure above is very simple and efficient and works well for many systems. Nevertheless, in the cases of absorptive layers, for which ϵ_j has an imaginary part, and for metallic systems or right above a resonance for dielectric systems, for which ϵ_j may be negative, the wavevector components k_j may become complex. This may be the case even for transparent systems in the case where Q is so large that the arguments of the square roots in Eq. (5) become negative. In this case, the trigonometric functions in the transfer matrix (Eq. (4)) get an exponential contribution. Upon the multiplication of many of them to get the transfer matrix of the whole system (Eq. (1)), all the matrix elements would grow exponentially with the size of the system, yielding extremely ill-conditioned matrices that may become useless for the accurate computation of optical properties.

We notice that even when there is dissipation, the transfer matrix of each layer ought to be unimodular, i.e., $\det \mathbf{M}_j = 1$ [19]. Thus, \mathbf{M} should also be unimodular and its two eigenvalues ought to be mutually inverse. Nevertheless, in the presence of dissipation, all elements of the transfer matrix would be large. Thus, there ought to be an exquisite cancellation of large terms in the determinant to yield the value 1. Small numerical noise would destroy this cancellation precluding the accurate calculation of the smallest eigenvalue.

An alternative to the procedure above is to use an extended or complete $2N \times 2N$ matrix [19] instead of a single 2×2 transfer matrix, in order to solve simultaneously the set of $2N$ equations (3) together with Eqs. (6) and (7) for r , t , and the fields $E_{\parallel}(z_j)$ and $H_{\parallel}(z_j)$ at all internal interfaces $j = 1 \dots N - 1$. Thus we solve an equation of the form

$$\mathbf{L}\mathbf{F} = \mathbf{I}, \quad (8)$$

where

$$\mathbf{F} = (r, E_{\parallel}(z_1), H_{\parallel}(z_1), \dots, E_{\parallel}(z_{N-1}), H_{\parallel}(z_{N-1}), t)^T \quad (9)$$

contains information about the field everywhere within the structure,

$$\mathbf{I} = (I_1, I_2, \dots, 0, 0)^T \quad (10)$$

is the inhomogeneous driving term, with

$$I_1 = \begin{cases} -m_{11}^1 - Y_0 m_{12}^1 & \text{(TE)} \\ -Z_0 m_{11}^1 - m_{12}^1 & \text{(TM)} \end{cases}, \quad I_2 = \begin{cases} -m_{21}^1 - Y_0 m_{22}^1 & \text{(TE)} \\ -Z_0 m_{21}^1 - m_{22}^1 & \text{(TM)} \end{cases}, \quad (11)$$

(we denote by the superscript T the transpose of a matrix) and

$$\mathbf{L} = \begin{pmatrix} \mathbf{L}_1 & -\mathbf{1}_{2 \times 2} & \mathbf{0}_{2 \times 2} & \mathbf{0}_{2 \times 2} & \cdots & \cdots & \cdots & \mathbf{0}_{2 \times 1} \\ \mathbf{0}_{2 \times 1} & \mathbf{M}_2 & -\mathbf{1}_{2 \times 2} & \mathbf{0}_{2 \times 2} & \cdots & \cdots & \cdots & \mathbf{0}_{2 \times 1} \\ \mathbf{0}_{2 \times 1} & \mathbf{0}_{2 \times 2} & \mathbf{M}_3 & -\mathbf{1}_{2 \times 2} & \cdots & \cdots & \cdots & \mathbf{0}_{2 \times 1} \\ \vdots & \vdots & \vdots & \vdots & \ddots & \ddots & \ddots & \vdots \\ \mathbf{0}_{2 \times 1} & \mathbf{0}_{2 \times 2} & \cdots & \cdots & \cdots & \mathbf{M}_{N-1} & -\mathbf{1}_{2 \times 2} & \mathbf{0}_{2 \times 1} \\ \mathbf{0}_{2 \times 1} & \mathbf{0}_{2 \times 2} & \cdots & \cdots & \cdots & \cdots & \mathbf{M}_N & \mathbf{L}_2 \end{pmatrix} \quad (12)$$

is a large sparse matrix coupling the field components among themselves, which we write in blocks, where $\mathbf{1}_{2 \times 2}$ is the unit 2×2 matrix, $\mathbf{0}_{2 \times 1}$ and $\mathbf{0}_{2 \times 2}$ are a 2×1 and 2×2 matrices of zeroes, and we defined

$$\mathbf{L}_1 = \begin{cases} (m_{11}^1 - Y_0 m_{12}^1, m_{21}^1 - Y_0 m_{22}^1)^T, & \text{(TE)} \\ (-Z_0 m_{11}^1 + m_{12}^1, -Z_0 m_{21}^1 + m_{22}^1)^T, & \text{(TM)} \end{cases} \quad (13)$$

$$\mathbf{L}_2 = \begin{cases} -(1, Y_s)^T, & \text{(TE)} \\ -(Z_s, 1)^T, & \text{(TM)} \end{cases}$$

where we denote by m_{kl}^j the k, l -th element of the matrix \mathbf{M}_j .

Many standard methods may be employed to solve Eq. (8), such as the Gaussian elimination [20, 21], Gauss-Jordan [22, 20], Choleski [23, 20], conjugate gradient [24, 20, 22], and generalized minimal residual methods [25, 20], among others. Some may take advantage for the sparseness and tridiagonality by blocks of the matrix of coefficients in Eq. (12), while others may not. In any case, these methods include pivoting strategies that judiciously choose the sequence of steps to take in simplifying the system of equations in order to numerically stabilize the solution procedure. The usual transfer matrix formalism is equivalent to an immediate elimination of all the fields $E_{\parallel}(z_j)$ and $H_{\parallel}(z_j)$, $j = 1 \dots N - 1$, which a priori may not turn out to be the best strategy with regards to the numerical stability of the solution. For this reason, we expect that the solution of Eq. (8) may be accurately obtained in systems for which that of Eqs. (2), (6) and (7) may not.

2.3 Bloch Expansion

In the previous subsection we presented a method for obtaining the optical coefficients of a layered structure together with the fields at all its interfaces, that we expect would be more stable than the common transfer matrix method of subsection 2.1. Nevertheless, it implies a much larger computational load. This may be a bagatelle for a single calculation, but it may be of importance, for example, when designing an optimized structure through a minimization procedure that requires full spectra to be calculated for all candidate sets of design parameters. For this reason, in this subsection we develop an alternative method.

To this end, we take the complete multilayered system of Fig. 1, and we replicate it periodically to form an infinite artificial photonic crystal. We can then use Bloch's theorem to describe the normal modes of this crystal. According to Bloch's theorem, the modes of a periodic system may be written as a superposition of Bloch waves, each of which acquires a *phase factor* as it propagates from one period to the next. Therefore, each Bloch wave would obey

$$\begin{pmatrix} E_{\parallel}^{\pm} \\ H_{\parallel}^{\pm} \end{pmatrix}_{z_N} = \mathbf{M} \begin{pmatrix} E_{\parallel}^{\pm} \\ H_{\parallel}^{\pm} \end{pmatrix}_{z_0} = e^{\pm iKD} \begin{pmatrix} E_{\parallel}^{\pm} \\ H_{\parallel}^{\pm} \end{pmatrix}_{z_0}, \quad (14)$$

where $D = z_N - z_0$ is the period, which corresponds to the actual thickness of the multilayered system, and $\pm K$ represents a 1D Bloch's vector corresponding to a wave that propagates along the $\pm z$ direction [26, 27, 28]. Thus, $\Lambda_{\pm} = e^{\pm iKD}$ are the eigenvalues of the transfer matrix \mathbf{M} and $(E_{\parallel}^{\pm}, H_{\parallel}^{\pm})^T$ are the corresponding eigenvectors. Notice that we have used the fact that $\det \mathbf{M} = 1$ exactly, so that the product of the eigenvalues is $\Lambda_+ \Lambda_- = 1$, and the dispersion relation of the Bloch modes may be obtained in principle from

$$\cos KD = \frac{1}{2} \text{tr} \mathbf{M}, \quad (15)$$

where tr denotes the trace.

Consider now a finite system of width MD made by stacking together M periods on a substrate. In this case, periodicity would be lost, and a single Bloch mode would not solve the electromagnetic wave problem. Nevertheless, the upwards moving Bloch wave would be reflected downwards at the interface with the substrate, and a downwards moving Bloch wave would be reflected upwards at the interface with the ambient. Thus, the optical properties of a finite system may be obtained by considering a wave incoming from the ambient, a wave reflected back towards the ambient, a wave transmitted towards the substrate and two Bloch waves within the multilayered system, one moving upwards and one moving downwards, as illustrated in Fig. 2 for the extreme case of only $M = 1$ period, which is the case we analyze below. The continuity of E_{\parallel} and H_{\parallel} would yield two equations at the two interfaces, with the ambient and with the substrate, from which we may obtain the four unknowns, namely, r , t and the amplitudes of both Bloch waves. Notice that for an infinite system,

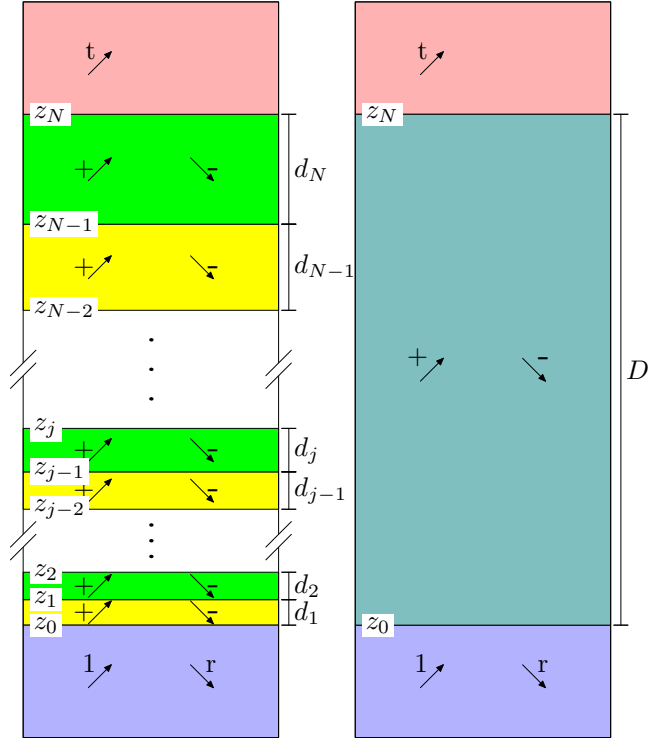


Figure 2: A wave of amplitude 1 is incident from the ambient into the surface of a multilayered system where it is partially reflected into the ambient and transmitted towards the substrate. Within each layer there are waves propagating upwards (+) and downwards (-). The multilayered system may be replaced by an effective wide layer within which there is one Bloch wave propagating upwards and another propagating downwards. The optical coefficients r and t and the amplitudes of the Bloch waves may be obtained by applying boundary conditions on E_{\parallel} and H_{\parallel} at z_0 and z_N .

Bloch's vector K should be real, as the Bloch wave would otherwise diverge either as $z \rightarrow \infty$ or $z \rightarrow -\infty$. Nevertheless, for a finite system we may use *Bloch-like* modes, for which we allow K to be complex.

In the presence of even a very tiny dissipation, the Bloch-like waves should decay as they propagate. Thus, we identify the eigenvalue of the upwards moving mode $\Lambda_+ = e^{iKD}$ as the one that obeys $|\Lambda_+| < 1$, $\text{Im}K > 0$, adding a negligible amount of dissipation if necessary to resolve the apparent ambiguity when $|\Lambda_+| = 1$. Similarly, the downwards moving wave has

$$|\Lambda_-| > 1. \quad (16)$$

Notice that we may avoid the numerical instability issues discussed above if we first identify the eigenvalue for the downwards wave

$$\Lambda_- = \frac{1}{2} \text{tr} \mathbf{M} \pm i \sqrt{1 - (\text{tr} \mathbf{M} / 2)^2}, \quad (17)$$

where we chose the sign so as to obey Eq. (16), and then obtain the eigenvalue for the upward wave

$$\Lambda_+ = \frac{1}{\Lambda_-}. \quad (18)$$

Following this procedure we avoid the cancellations which amplify the numerical noise and we obtain eigenvalues that are consistent with the exact unimodularity of the transfer matrix.

Having obtained the eigenvalues Λ_{\pm} of the transfer matrix, we may obtain the corresponding eigenvectors E_{\parallel}^{\pm} and H_{\parallel}^{\pm} from Eq. (14), and from them, the corresponding surfaces impedances

$$Z^{\pm} = -\frac{M_{12}}{M_{11} - \Lambda_{\pm}}, \quad (19)$$

where M_{ij} ($i, j = 1, 2$) denote the elements of the transfer matrix \mathbf{M} . By writing the fields at z_0 and z_N as a superposition of upward and downward propagating (or decaying) fields $E_{\parallel}^{\pm} = Z^{\pm} H_{\parallel}^{\pm}$, we can relate the fields at z_N to the fields at z_0 through a *reconstructed* transfer matrix,

$$\begin{pmatrix} E_{\parallel} \\ H_{\parallel} \end{pmatrix}_{z_N} = \tilde{\mathbf{M}} \begin{pmatrix} E_{\parallel} \\ H_{\parallel} \end{pmatrix}_{z_0}, \quad (20)$$

where

$$\tilde{\mathbf{M}} = \frac{1}{Z^+ - Z^-} \begin{pmatrix} Z^+ \exp(iKD) - Z^- \exp(-iKD) & -2iZ^+Z^- \sin KD \\ 2i \sin KD & Z^+ \exp(-iKD) - Z^- \exp(iKD) \end{pmatrix}. \quad (21)$$

It can be shown that this matrix complies with unimodularity.

The result above can be readily generalized to a system of MN layers made up of $M > 1$ repetitions of an arbitrary structure with N layers. To that end it is only necessary to interpret \mathbf{M} in Eqs. (15) and (17) as the transfer matrix of one period, substitute z_N by z_{MN} in Eq. (20) and D by MD in Eq. (21).

We can finally solve Eqs. (6), (7), (20) and (21) to obtain explicit expressions for the optical coefficients

$$r = \mp \frac{Z_0 \tilde{M}_{11} + \tilde{M}_{12} - Z_0 Z_s \tilde{M}_{21} - Z_s \tilde{M}_{22}}{Z_0 \tilde{M}_{11} - \tilde{M}_{12} - Z_0 Z_s \tilde{M}_{21} + Z_s \tilde{M}_{22}}, \quad (22)$$

and

$$t = \frac{2Z_\alpha}{Z_0 \tilde{M}_{11} - \tilde{M}_{12} - Z_0 Z_s \tilde{M}_{21} + Z_s \tilde{M}_{22}}, \quad (23)$$

where we choose the upper sign $-$ in Eq. (22) and the subscript $\alpha = s$ in Eq. (23) for the case of TE polarization, while the lower sign $+$ and the subscript $\alpha = 0$ correspond to TM polarization. As usual, the reflectance is given by $R = |r|^2$ and the transmittance by $T = \beta |t|^2$ with $\beta = Z_0/Z_s$ for the case of TE polarization and $\beta = Z_s/Z_0$ for the case of TM polarization. Notice that one may factor out and cancel from Eq. (22) a possibly large factor e^{-iKD} and that the dominant term when $\text{Im } KD$ is large is

$$r \approx \pm \frac{Z^+ - Z_0}{Z^+ + Z_0}, \quad (24)$$

which coincides with the result for a semi-infinitely repeated system, as there would be a negligible contribution from the Bloch-like wave reflected at the substrate. In this case, instead of starting the calculation above from \mathbf{M} it may be enough to start from a partial transfer matrix

$$\mathbf{M}' = \mathbf{M}_{N'} \mathbf{M}_{N'-1} \dots \mathbf{M}_2 \mathbf{M}_1 \quad (25)$$

with $N' < N$, but large enough so that the interface at $z_{N'}$ is beyond the reach of the upward-moving Bloch's wave.

3 Experimental details

A photonic structure was synthesized through anodic etching of a (100) oriented, p-type Boron doped, crystalline Si wafer with resistivity 0.002-0.005 $\Omega \cdot \text{cm}$, under galvanostatic conditions [29, 11]. The electrochemical anodizing process was performed at room temperature, with an electrolyte mixture of aqueous HF (48% (w/w)) and ethanol (99.9% (w/w)) in 1:1 volumetric proportion, respectively. The current density and the etching duration of each layer was controlled using a programmable current source. The current densities were chosen as 2 and 305 mA/cm^2 , with corresponding porosities 41% and 76%, respectively. The calibration curves were acquired through a gravimetric technique as follows: Silicon wafers were used for synthesizing under similar conditions single layers of porous silicon, their weights m_i were determined before (m_1) and after (m_2) the electrochemical attack, and after dissolving the already formed porous silicon layer (m_3), to calculate the porosity as $p = (m_1 - m_2)/(m_1 - m_3)$ [30]. The rate of formation of the nanostructured porous silicon films was obtained

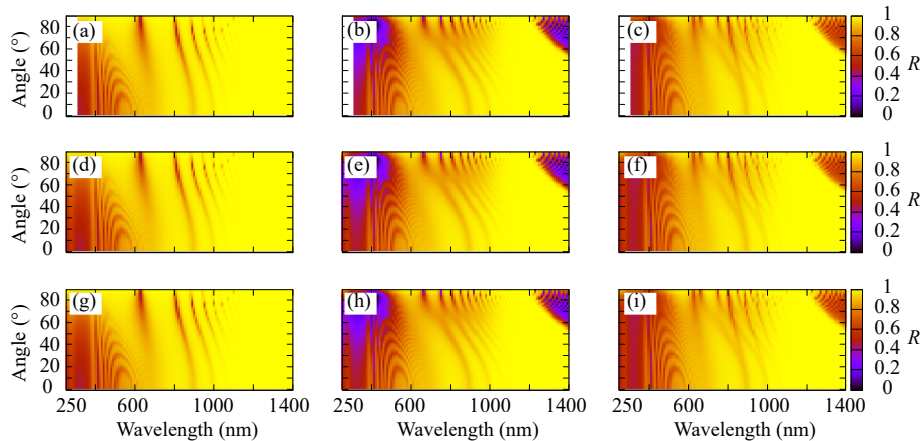


Figure 3: Reflectance spectra of a structure of 101 pairs of PS layers, calculated as a function of angle of incidence θ_i and wavelength λ using the transfer matrix (upper panels), the extended matrix (middle), and the Bloch expansion methods (lower) for TE (left), and TM (center) polarizations, and for non-polarized light (right). The layers have porosities $p_1 = 41\%$ and $p_2 = 76\%$ and widths obtained from Eqs. (26) and (27) choosing $\lambda_i = 400$ nm, $\lambda_f = 1400$ nm and $\nu = 0.35$.

by synthesizing again single layers under similar conditions and measuring their thicknesses through scanning electron microscopy (SEM). The absolute reflectivity measurements were carried out with a Perkin Elmer Lambda 950 UV/Visible spectrophotometer with a variable angle universal reflectance accessory (URA) for different incident angles $\theta_i = 8^\circ, 30^\circ, 45^\circ$ and 60° using non-polarized light. The maximum and minimum values of θ_i were constrained by the angular range of the URA.

4 Results and discussion

In Fig. 3 we show the reflectance spectra calculated with the three methods discussed in Sec. 2 for a system made up of $P = 101$ pairs of PS layers with alternating porosities $p_1 = 41\%$ and $p_2 = 76\%$ respectively on a Si substrate. The thicknesses d_{2k-1} and d_{2k} ($k = 1 \dots P$) were chosen to correspond to quarter-wave plates,

$$k_{2k-1}^D d_{2k-1} = k_{2k}^D d_{2k} = \pi/2, \quad (26)$$

as in a *Bragg mirror* [8, 16], where k_{2k-1}^D and k_{2k}^D were obtained from Eq. (5) evaluated at a given depth dependent *design* wavelength [6]

$$\lambda_k^D = \lambda_i + (\lambda_f - \lambda_i) \left(\frac{k-1}{P-1} \right)^\nu \quad (27)$$

with initial wavelength $\lambda_i = 400$ nm and final wavelength $\lambda_f = 1400$ nm. The value of the exponent $\nu = 0.35$ was chosen by maximizing the calculated reflectance averaged over the wavelengths 250 nm-1400 nm and the angles $0^\circ - 90^\circ$, respectively. To that end, we used the Nelder-Mead [31, 32] *simplex* method through the MINUIT package [33]. This is a widely used simple but robust optimization algorithm. The optimal average reflectance we obtained was 0.91. Eq. (27) has been shown to yield *chirped* multilayered structures with high reflectance over a wide frequency range [6]. The refractive indices of the nanostructured PS layers were obtained for each wavelength using the Bruggeman effective medium theory [30] and a wavelength dependent Si response [34, 35]. We notice that using the 2×2 transfer matrix, the reflectance spectra could not be calculated for wavelengths $\lambda < 310$ nm for which Si becomes highly dissipative and the double-precision transfer matrix overflowed numerically (white regions in upper row of Fig. 3).

The results of the extended matrix method coincide closely with those of the standard transfer matrix where the latter converges. Furthermore, it converges with no problem over all the range explored, down to and beyond $\lambda = 250$ nm. The results of using the Bloch expansion method are indistinguishable from those of the extended matrix. Thus, despite the fact that the standard transfer matrix method is very useful and commonly used, it fails when the system is highly dissipative or is made up of a very large number of layers. The extended matrix and the Bloch expansion methods do not have this limitation. Moreover, they coincide among themselves and coincide with the transfer matrix method whenever it converges. Although numerical stability is obtained when working with the extended matrix, the computation time it requires is much larger than that of the 2×2 matrices. The time may be somewhat reduced by reducing the number of unknowns by aggregating the layers in groups characterized by a single matrix, given by the product of the transfer matrices of its members, as numerous as possible as long as that the determinant of the transfer matrix of the group does not drift away from the nominal value 1. Even applying this grouping separately for the spectral region where Si is highly dissipative, requiring many small groups, and where it is not, for which a few large groups suffice, the computation time required is much larger than that using the Bloch expansion. Thus, we conclude that the Bloch expansion provides us with numerical stability, reliability and computational efficiency. An advantage, though, of the extended matrix, is that it yields the field profiles, as illustrated below.

In Fig. 4 we show the squared magnitude of the electric field as a function of depth for the case of a TE field incident on the same structure as in Fig. 3 for various angles of incidence and wavelengths, obtained by using the extended matrix. We observe that the penetration depth of the electromagnetic field increases as the wavelength increases. This is not unexpected, as we designed our structure with thicker layers deeper inside. The penetration depth also increases as the angle of incidence increases. Notice the oscillations in the field profile, more notable for the cases with deeper penetration. There are short lengthscale oscillations corresponding to the texture of the structure, and longer lengthscale oscillations due to the interference between multiply reflected waves from the

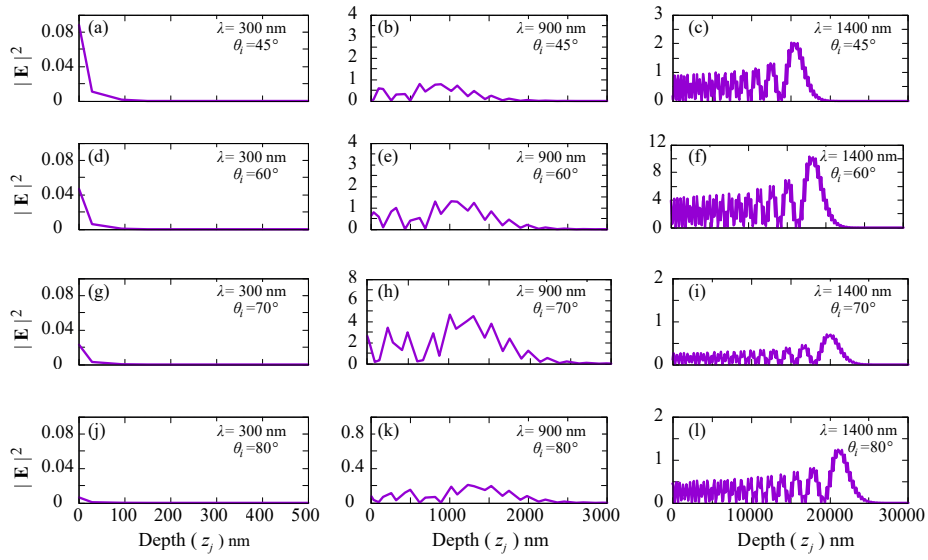


Figure 4: Squared magnitude of the electric field for TE polarization as a function of depth for same system as in Fig. 3 for different angles of incidence ($\theta_i = 45^\circ, 60^\circ, 70^\circ,$ and 80° from top to bottom) and several wavelengths ($\lambda = 300$ nm, 900 nm, and 1400 nm from left to right).

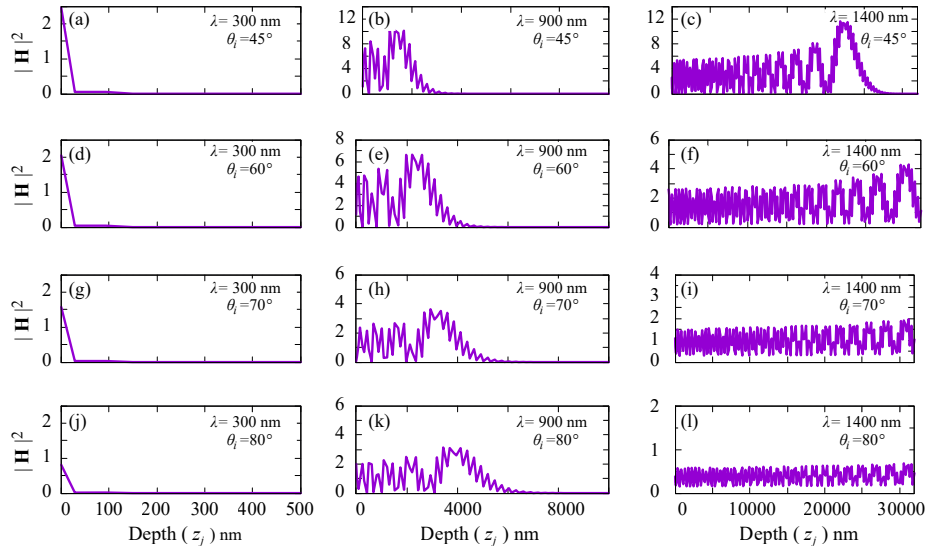


Figure 5: Squared magnitude of the magnetic field as a function of depth, as in Fig. 4, but for TM polarization.

region where propagation is forbidden due to Bragg reflections and from the front surface of the structure. These long-scale oscillations are responsible for the oscillations visible in the reflectance spectra for long wavelengths in Fig. 3.

We remark that while the total thicknesses of this structure is $D \approx 32 \mu\text{m}$, the penetration depth turns out to be no larger than $25 \mu\text{m}$, covering just 83 of the 101 periods, in the case $\lambda = 1400 \text{ nm}$, $\theta_i = 80^\circ$.

In the corresponding case but for TM polarization, the field penetrates a much larger distance, as shown Fig. 5 for the same structure as in Fig. 4. In this case, the field already penetrates more than $25 \mu\text{m}$ for $\lambda = 1400 \text{ nm}$ and $\theta_i = 45^\circ$, while for larger angles it penetrates the entire structure.

The results above suggest that for some combinations of polarization, wavelength and angle of incidence, smaller structures may produce the same results than the full structures discussed previously. In Fig. 6 we show the reflectance spectra calculated for TE and TM polarizations, and for non-polarized light using the Bloch expansion for a multilayered system consisting of the first 83 periods of the system corresponding to Fig. 3 with 101 periods. According to Fig. 4, this system is wider than the penetration depth for TE polarization and $\theta_i < 80^\circ$ and we can observe the expected correspondence between Figs. 6a-c with Figs. 3g-i. We have verified this agreement quantitatively. The agreement for TE polarization is better than for TM, given the smaller penetration depth. Even though we considered here narrower systems, the usual transfer matrix method failed in the UV, while the extended matrix and the Bloch expansion methods succeeded and were consistent.

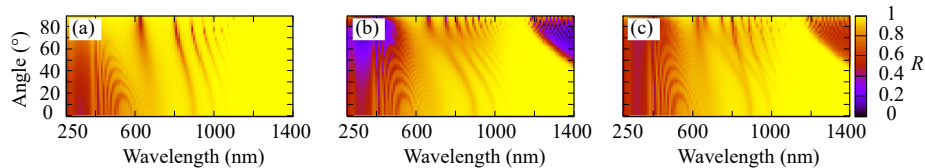


Figure 6: Reflectance spectra as a function of wavelength and angle of incidence obtained for TE (left), TM (center) polarizations, and for non-polarized light (right), using the Bloch expansion for a structure as in Fig. 3 but with only the first 83 periods.

In Fig. 7 we show the experimental reflectance for non-polarized incident light as a function of wavelength for various angles of incidence. The fabricated sample corresponds to the structure presented in Fig. 3, and consists of 101 pairs of layers with target porosities 41% and 76%, as described in Sec. 3, and with target widths obtained from Eqs. (26) and (27) with $\lambda_i = 400$ nm, $\lambda_f = 1400$ nm and $\nu = 0.35$. SEM images of the synthesized structure are also shown in the figure, displaying the gradual increase in the thickness of the layers with increasing depth. For comparison, Fig. 7 also shows theoretical results obtained as in Fig. 3. Notice that we could calculate R for the lowest wavelengths only through our proposed formalisms. The calculated and measured spectra have similar features, though the experimental reflectance is lower, more so at larger angles, and their differences are also larger at shorter wavelengths, where the theoretical reflectance shows larger oscillations. The differences between the experimental and calculated spectra could be partially due to the scattering of light at the actual interfaces, which naturally have some roughness [36]. They may also be due to confinement induced changes in the dielectric function of the Si phase of porous silicon, as it has been argued [37, 38] that in the blue spectral range the imaginary part of the response of the solid phase of heavily p-type doped porous silicon is significantly larger than that of bulk silicon, and that its interband transitions become broadened and red-shifted. Thus, in Fig. 7 we also show theoretical results obtained as in Fig. 3 but incorporating some effects of roughness through a macroscopic interface transfer matrices [36] and convoluting the dielectric function of the Si phase [34, 35] with a Gaussian weight in order to red-shift and broaden its spectral features. The parameters of the modified theory are the roughness height, and the red-shift and broadening of the Si response. Thus, we fitted a shift of $0.032 \mu\text{m}$ and a spectral broadening of $0.022 \mu\text{m}$, of the order of those discussed in Refs. [37, 38], and a depth dependent roughness amplitude that increases grows from 0.5 to 2.6 nm from ambient towards substrate in proportion to the widths of each layer. The modified theory yields a lower reflectance overall, diminished oscillations for short wavelengths and the decay of the reflectance of large wavelengths and large angles, in good agreement with experiment. In Fig. 7 we also illustrate the profile of the structure through a SEM image. The gradual increase of the thickness of the

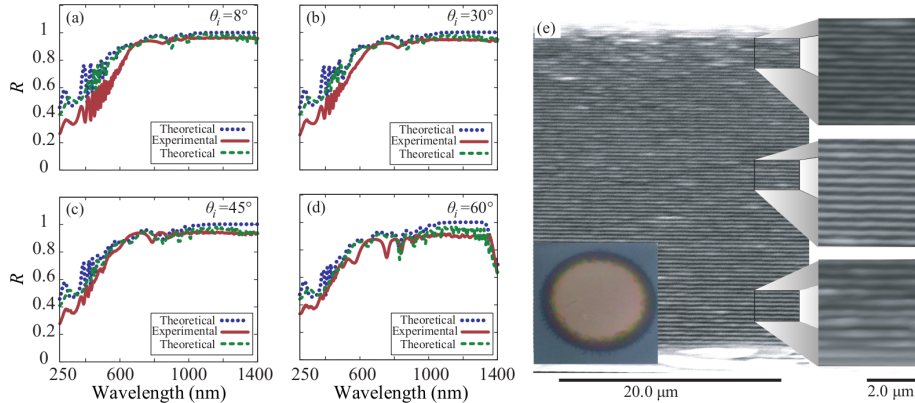


Figure 7: Measured (solid red) and calculated (dotted blue) reflectivity spectra of the sample described in the text as a function of wavelength at four different angles (a) 8° , (b) 30° , (c) 45° and (d) 60° . We also include a modified calculation that accounts for some roughness and confinement effects (green dashed, see text). (e) Micrograph of the cross-section of the 101-period structure. The inset shows a top view photograph.

layers with increasing depth is visible and is consistent with our design given by Eq. (27).

5 Conclusions

We have shown that the usual transfer matrix approach to the calculation of optical properties of multilayered systems may fail for large systems in the presence of absorption. Nevertheless, numerical stability may be achieved by using 2 alternative methods: using an extended or complete transfer matrix and using a method based on the excitation of Bloch-like modes. We applied these methods to the calculation of the reflectance spectrum of a wide spectrum omnidirectional mirror consisting of a large multilayered chirped structure made of porous silicon. Both proved to be precise and stable. The extended matrix is considerably slower than the expansion in Bloch modes, but it yields more information and allows an analysis of the fields dependence on depth, which we applied to study the wavelength and angle dependent penetration depth, which in turn allowed us to replace the original structures by a thinner one that yielded the desired optical properties within a large range of wavelengths and angles of incidence. On the other hand, the expansion in Bloch-like modes allows fast, stable and accurate calculations, providing thus an ideal method for the design and optimization of large multilayered structures which could be made of periodic repetitions of a single unit or completely aperiodic as in our chirped example. We compared our calculated reflectance spectra to experimen-

tal results and obtained good agreement even for the UV region where there is relatively strong absorption. The agreement could be improved by considering effects such as the interfacial roughness and the modification of the response of Si within the confined pore walls, effects that can readily be incorporated into our formalism. Thus, we conclude that our approach is useful for the computation, design and analysis of the optical properties of very large multilayered systems.

Acknowledgments

This work was supported by DGAPA-UNAM under grant IN111119 and by CONACyT under grant A1S-30393. LEPD and VCG acknowledge a scholarship from CONACyT. GPO acknowledges the support of ANPCyT-FONCyT through grant PICT-0696-2013 and SGCyT-UNNE through grants PI-F008-2014 and PI-18F008. HPA also express his gratitude to the *Coordinación de la Investigación Científica de la Universidad Michoacana de San Nicolás de Hidalgo*. VCG acknowledges useful discussions with A. David Ariza-Flores.

References

- [1] Yoel Fink, Joshua N. Winn, Shanhui Fan, Chiping Chen, Jurgen Michel, John D. Joannopoulos, and Edwin L. Thomas. A dielectric omnidirectional reflector. *Science*, 282(5394):1679–1682, 1998.
- [2] John Lekner. Omnidirectional reflection by multilayer dielectric mirrors. *J. Opt. A: Pure Appl. Opt.*, 2(5):349–352, 2000.
- [3] Joshua N. Winn, Yoel Fink, Shanhui Fan, and J. D. Joannopoulos. Omnidirectional reflection from a one-dimensional photonic crystal. *Opt. Lett.*, 23(20):1573–1575, 1998.
- [4] Lin Weihua, Wang Guo Ping, and Zhang Suhuai. Design and fabrication of omnidirectional reflectors in the visible range. *J. Mod. Opt.*, 52(8):1155–1160, 2005.
- [5] Guan Huihuan, Han Peide, Yang Yanqing, Li Yuping, Zhang Xue, and Zhang Wenting. Omni-directional mirror for visible light based on one-dimensional photonic crystal. *Chin. Opt. Lett.*, 9(7):071603–071603, 2011.
- [6] A. David Ariza-Flores, L. M. Gaggero-Sager, and V. Agarwal. White metal-like omnidirectional mirror from porous silicon dielectric multilayers. *Appl. Phys. Lett.*, 101(3):031119, 2012.
- [7] S. Jena, R.B. Tokas, P. Sarkar, J.S. Misal, S. Maidul Haque, K.D. Rao, S. Thakur, and N.K. Sahoo. Omnidirectional photonic band gap in magnetron sputtered tio2/sio2 one dimensional photonic crystal. *Thin Solid Films*, 599:138–144, 2016.

- [8] Bruyant A., G. Léronde, P. J. Reece, and M. Gal. All-silicon omnidirectional mirrors based on one-dimensional photonic crystals. *Appl. Phys. Lett.*, 82(19):3227–3229, 2003.
- [9] Yeonsang Park, Young-Geun Roh, Chi-O Cho, Heonsu Jeon, Min Gyu Sung, and J. C. Woo. Gaas-based near-infrared omnidirectional reflector. *Applied Physics Letters*, 82(17):2770–2772, 2003.
- [10] Sreeramulu Valligatla, Alessandro Chiasera, Stefano Varas, Nicola Bazzanella, D. Narayana Rao, Giancarlo C. Righini, and Maurizio Ferrari. High quality factor 1-d er3+-activated dielectric microcavity fabricated by rf-sputtering. *Opt. Express*, 20(19):21214–21222, 2012.
- [11] J. Escorcía and V. Agarwal. Effect of duty cycle and frequency on the morphology of porous silicon formed by alternating square pulse anodic etching. *Phys. Status Solidi (c)*, 4(6):2039–2043, 2007.
- [12] A. David Ariza-Flores, L. M. Gaggero-Sager, and V. Agarwal. Effect of interface gradient on the optical properties of multilayered porous silicon photonic structures. *Journal of Physics D: Applied Physics*, 44(15):155102, 2011.
- [13] J. O. Estevez, J. Arriaga, Méndez Blas A, and Agarwal V. Omnidirectional photonic bandgaps in porous silicon based mirrors with a gaussian profile refractive index. *Appl. Phys. Lett.*, 93(19):191915, 2008.
- [14] J. O. Estevez, J. Arriaga, A. Méndez Blas, and V. Agarwal. Enlargement of omnidirectional photonic bandgap in porous silicon dielectric mirrors with a gaussian profile refractive index. *Appl. Phys. Lett.*, 94(6):061914, 2009.
- [15] E. Xifré-Pérez, L. F. Marsal, J. Pallarès, and J. Ferré-Borrull. Porous silicon mirrors with enlarged omnidirectional band gap. *Journal of Applied Physics*, 97(6):064503, 2005.
- [16] E. Xifré-Pérez, L. F. Marsal, J. Ferré-Borrull, and J. Pallarès. Low refractive index contrast porous silicon omnidirectional reflectors. *Applied Physics B*, 95(1):169–172, 2009.
- [17] P. Yeh. *Optical Waves in Layered Media*. Wiley, USA, 2nd edition, 2005.
- [18] David. Ariza-Flores, L. M. Gaggero-Sager, and V. Agarwal. Omnidirectional photonic bangap in dielectric mirrors: a comparative study. *Journal of Physics D: Applied Physics*, 45(1):015102, 2011.
- [19] R. Perez-Alvarez and F. Garcia-Molina. *Transfer Matrix, Green Functions and Related Techniques*. Castello de la Plana: Publicacions de la Universitat Jaume I, 2004.
- [20] J. Stoer and R. Bulirsch. *Introduction to Numerical Analysis*. Springer, NewYork, 3rd edition, 1993.

- [21] Markus Olschowka and Arnold Neumaier. A new pivoting strategy for gaussian elimination. *Linear Algebra and its Applications*, 240:131–151, 1996.
- [22] J. H. Wilkinson and C. Reinsch. *Handbook for Automatic Computation: Volume II: Linear Algebra*. Springer-Verlag Berlin Heidelberg, New York, 1st edition, 1971.
- [23] David S. Kershaw. The incomplete cholesky—conjugate gradient method for the iterative solution of systems of linear equations. *Journal of Computational Physics*, 26:43–65, 1978.
- [24] M. R. Hestenes and E. Stiefel. Methods of conjugate gradients for solving linear systems. *J. of Res. Nat. Bur. Standards*, 49:409–436, 1952.
- [25] Youcef Saad and Martin H. Schultz. Gmres: A generalized minimal residual algorithm for solving nonsymmetric linear systems. *SIAM J. Sci. and Stat. Comput.*, 7(3):856–869, 1986.
- [26] J. S. Pérez-Huerta, D. Ariza-Flores, R. Castro-García, W. L. Mochán, G. P. Ortiz, and V. Agarwal. Reflectivity of 1D photonic crystals: A comparison of computational schemes with experimental results. *Int. J. Mod. Phys. B*, 32(11):1850136, 2018.
- [27] W. Luis Mochán, Marcelo del Castillo-Mussot, and Rubén G. Barrera. Effect of plasma waves on the optical properties of metal-insulator superlattices. *Phys. Rev. B*, 35(3):1088–1098, 1987.
- [28] W. Luis Mochán and Marcelo del Castillo-Mussot. Optics of multilayered conducting systems: Normal modes of periodic superlattices. *Phys. Rev. B*, 37(12):6763–6771, 1988.
- [29] Canham L. T. Silicon quantum wire array fabrication by electrochemical and chemical dissolution of wafers. *Appl. Phys. Lett.*, 57(10):1046–1048, 1990.
- [30] Pap Andrea Edit, Kordás Krisztián, Vähäkangas Jouko, Uusimäki Antti, Leppävuori Seppo, Pilon Laurent, and Szatmári Sándor. Optical properties of porous silicon. part iii: Comparison of experimental and theoretical results. *Optical Materials*, 28(5):506–513, 2006.
- [31] J. A. Nelder and R. Mead. A simplex method for function minimization. *The Computer Journal*, 7:308–313, 1965.
- [32] Jeffrey C. Lagarias, James A. Reeds, Margaret H. Wright, and Paul E. Wright. Convergence properties of the nelder–mead simplex method in low dimensions. *SIAM J. Optim.*, 9(1):112–147, 1998.
- [33] F. James and M. Winkler. *Minuit user’s guide*. CERN, Geneva, 2004.

- [34] E.D. Palik. *Handbook of Optical Constants of Solids*. Elsevier, 1998.
- [35] Carsten Schinke, P. Christian Peest, Jan Schmidt, Rolf Brendel, Karsten Bothe, Malte R. Vogt, Ingo Kröger, Stefan Winter, Alfred Schirmacher, Siew Lim, Hieu T. Nguyen, and Daniel MacDonald. Uncertainty analysis for the coefficient of band-to-band absorption of crystalline silicon. *AIP Advances*, 5(6):067168, 2015.
- [36] Guillermo P. Ortiz, J Victor J. Toranzos, Leandro A. Missoni, María L. Martínez-Ricci, and W. Luis Mochán. Rough 1D photonic crystals: a transfer matrix approach. Submitted to *Journal of Optics*. arxiv:2004.00185 [physics.optics].
- [37] W. Theiß, R. Arens-Fischer, M. Arntzen, M.G. Berger, S. Frohnhoff, S. Hilbrich, and Wernke M. Probing optical transitions in porous silicon by reflectance spectroscopy in the near infrared, visible and UV. *MRS Proceedings*, 358:435, 1994.
- [38] W. Theiß. Optical properties of porous silicon. *Surface Science Reports*, 29(3):91–192, 1997.